Structure, Composition, and Morphology of Photoelectrochemically Active $TiO_{2-x}N_x$ Thin Films Deposited by Reactive DC Magnetron Sputtering

Julius M. Mwabora,[†,‡] Torbjörn Lindgren,[†] Esteban Avendaño,[†] Thomas F. Jaramillo,[§] Jun Lu,[†] Sten-Eric Lindquist,[||] and Claes-Göran Granqvist*[,†]

Department of Engineering Sciences, The Ångström Laboratory, Uppsala University, P. O. Box 534, SE-751 21 Uppsala, Sweden, Department of Chemical Engineering, University of California, Santa Barbara, California 93106-5080, and Department of Physical Chemistry, Uppsala University, P. O. Box 532, SE-751 21 Uppsala, Sweden

Received: September 29, 2003; In Final Form: August 23, 2004

Films of nitrogen-doped TiO_2 were made by reactive DC magnetron sputtering in a mixture of argon, oxygen, and nitrogen. The nitrogen gas ratio Φ was varied in the $0 < \Phi < 0.025$ range during the depositions, resulting in $TiO_{2-x}N_x$ films with $0 \leq x \leq 0.022$ as determined by X-ray photoelectron spectroscopy. Structural and morphological properties of the films were investigated by X-ray diffraction, atomic force microscopy, and scanning and transmission electron microscopy. Films prepared without nitrogen had a rutile structure, while the nitrogen-doped films were either rutile or anatase depending on Φ being below or above $\sim$0.007. Deposition rate, effective grain size, root-mean-square roughness, morphology, and optical absorption were also found to depend on Φ. The films were photoelectrochemically active, as reported in an earlier papers of ours [*J. Phys. Chem. B* **2003**, *107*, 5709−5716 and *J. Phys. Chem. B* **2004**, *108*, 5995−6003].

I. Introduction

Films of titanium dioxide, TiO_2, have attracted much interest during the past years owing to their many applications. Recent work has been reported on photoelectrochemical solar cells,[1,2] sensors,[3,4] electrochromic displays,[5] optical devices,[6] and collectors for photolysis of water, organics, and bacteria.[7−11] Other applications take advantage of the hydrophilicity of TiO_2.[12−14] At present, TiO_2 thin films for photoelectrochemical and photocatalytic applications are mainly produced by sol−gel processes[15] but magnetron sputtering is attracting increasing interest.[7,16−21] Sputtering can be used to fabricate large-scale uniform coatings and is industrially viable. It employs a nonequilibrium process, and external deposition conditions and internal plasma parameters can be used to optimize the film characteristics, such as crystalline phase, chemical composition, microstructure, and surface morphology.

With regard to photoelectrochemical and photocatalytic applications, it is of great interest to broaden the photoresponse of TiO_2 to also include the fraction of visible light in the solar spectrum. Traditionally, this has been achieved by anchoring organic dyes to the surface, and this approach has been successful in dye sensitized solar cells.[22] However, the commonly used ruthenium-based organic dyes are expensive and, moreover, the long-term stability of many dyes can be questioned. Another problem with organic dyes is that they can detach from the surface when employed in an aqueous solution. Therefore, there is a need to increase the photoactive spectrum by other approaches. Doping has been considered one alternative to design so-called "second-generation TiO_2 photocatalysts",[23] which can operate under visible light.

Already in 1986, Sato[24] reported on the photocatalytic activity in visible light for TiO_2 prepared and calcinated with NH_4OH. However, it took almost 15 years from then until nitrogen-doped TiO_2 was considered for photocatalytic applications. It was reported that nitrogen-doped TiO_2 (i.e., $TiO_{2-x}N_x$) shows a narrower band gap and a better photocatalytic activity under visible light than the corresponding undoped TiO_2.[7,25] Asahi et al.[7] prepared films by sputtering from a TiO_2 target in a mixture of Ar and N_2 and annealed the ensuing films at 550 °C for 4 h to obtain a mixed structure of crystalline anatase and rutile.

Apart from photocatalytic applications, titanium oxynitrides have received increasing attention over the past years for uses in protective coatings, electrical contacts, and diffusion barriers.[26] Many different preparation methods for titanium oxynitrides can be found in the literature; work has been reported on chemical vapor deposition,[26−28] physical vapor deposition (mainly sputtering),[7,9,29−34] and chemical methods.[7,10,24,35,36]

Our present work reports on nitrogen-doped TiO_2 films produced by reactive DC magnetron sputtering without post-treatment. Microstructural and morphological studies were carried out as a function of nitrogen content in the sputter gas by use of X-ray diffraction (XRD), scanning electron microscopy (SEM), transmission electron microscopy (TEM), atomic force microscopy (AFM), and X-ray photoelectron spectroscopy (XPS). Some complementary optical data are reported as well. The present paper is the third in a triology on nitrogen-doped TiO_2 where two previous ones have been specifically focused on photoelectrochemistry.[9,37]

II. Experimental Section

A. Film Preparation. The films were deposited by reactive DC magnetron sputtering in a system based on a Balzers UTT

* To whom correspondence should be addressed. E-mail: claes-goran.granqvist@angstrom.uu.se.
[†] Department of Engineering Sciences, Uppsala University.
[‡] Present and permanent address: Department of Physics, University of Nairobi, P.O. Box 30197, Nairobi, Kenya.
[§] University of California, Santa Barbara.
[||] Department of Physical Chemistry, Uppsala University.

10.1021/jp0368987 CCC: $27.50
Published on Web 12/01/2004

400 vacuum chamber.[38] The targets were 5-cm-diameter metallic plates of Ti (99.9% pure). The chamber was first evacuated to $\sim 10^{-7}$ Torr by turbo molecular pumping. Argon gas was then introduced, and the chamber was heated so that a stabilized substrate temperature of 250 ± 10 °C was accomplished. The Ti target was presputtered in argon for 5 min to remove surface oxides, and a subsequent presputtering was conducted for 5 min in a mixture of Ar, O_2, and N_2. The nitrogen gas flow ratio, Φ, was kept constant during the deposition by mass-flow-controlled gas inlets; it is defined as

$$\Phi = f(N_2)/f \tag{1}$$

where f is the total flow rate, that is,

$$f = f(O_2) + f(Ar) + f(N_2) \tag{2}$$

and $f(O_2)$, $f(Ar)$, and $f(N_2)$ are the individual flow rates of the gases. The $f(O_2)/f(Ar)$ gas flow ratio, Γ, was kept at a constant value of 0.06, while the total gas pressure was maintained at ~12 mTorr. Below, we refer to Φ as the "nitrogen ratio". The sputter plasma was generated at a constant current of 0.75 A. The power density, defined as the recorded power divided by the target area, was 17.4 W/cm^2 in the absence of nitrogen; it increased monotonically with increasing N_2 admixture and reached 19.3 for Φ being 0.025. Film uniformity was assured by rotating the substrate during deposition. After deposition, the films were cooled in Ar atmosphere for 1 h.

The substrates were supplied by Hartford glass (type Tec 8; thickness 1.5 mm) and had a transparent and conducting layer of fluorine-doped tin oxide with a sheet resistance of 8 Ω/square. The substrates were 5 × 5 cm^2 in size; they were cleaned immediately before each deposition by degreasing in a warm soap solution, further rinsing in deionized water, ultrasonic cleaning in ethanol, and drying in a stream of nitrogen gas. Corning 7059 glass substrates were used for optical characterization.

B. Film Characterization. Deposition rate r was determined by dividing film thickness, d, by deposition time. The thickness for all films was around 0.85 ± 0.05 μm, as measured by surface profilometry using a Tencor Alpha-Step 200 instrument on films taken out of the deposition system. The nitrogen-doped electrodes were bright yellow, transparent, and slightly light scattering. They were mechanically and thermally stable under the experimental conditions used. As a quick stability test, a film of nitrogen-doped rutile TiO_2 was annealed in an open atmosphere at 500 °C for 1 h without any noticeable change in the optical or photoelectrochemical properties.

The crystal structure was determined by XRD, using a Siemens D5000 diffractometer operating with Cu−K_α radiation. A grazing incidence setup was employed in parallel beam geometry for diffraction angles 2θ between 20 and 60 degrees. The effective grain size L_{eff} was estimated from Scherrer's formula,[39] that is,

$$L_{eff} = 0.9\lambda_{CuK\alpha}/(\beta \cos \theta) \tag{3}$$

where $\lambda_{CuK\alpha}$ is the X-ray wavelength and β is the full width at half-maximum of the diffraction peak.

Spectral normal transmittance $T(\lambda)$ and near-normal reflectance $R(\lambda)$ were measured using a Perkin-Elmer Lambda 900 spectrophotometer fitted with a 150-mm-diameter integrating sphere. Solar and luminous optical data were derived by averaging over the sun's AM1 spectrum ("air mass one", pertaining to the sun at zenith)[40] and the sensitivity of the light-adapted human eye,[40] respectively.

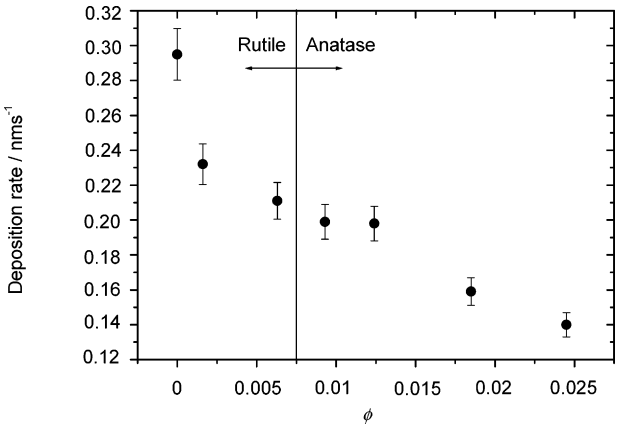

Figure 1. Deposition rate for nitrogen-doped titanium oxide films versus nitrogen content Φ in the sputter plasma. The vertical line indicates the demarcation between different crystal structures.

Optical absorption coefficient α was calculated from

$$\alpha(\lambda) = \frac{1}{d} \times \ln\left(\frac{1 - R(\lambda)}{T(\lambda)}\right) \tag{4}$$

The approximation applies when the refractive index of the substrate is between 1.5 and 1.7 and the refractive index of the coating is between 1.3 and 2.5. The approximation gives a relative error around 10% and a maximum relative error less than 15% for high refractive indices of the coatings.[41]

XPS was used to determine the stoichiometry of the $TiO_{2-x}N_x$ films. Specifically, a monochromated Al K_α source (1486.6 eV) was used with an eight-channel detector (Kratos, Axis Ultra). Samples were analyzed in as-deposited state, and Ar sputtering was not used so that preferential etching of light elements was avoided. During measurements, the pressure in the analytical chamber was approximately 2.0 × 10^{-9} Torr. Spectra were calibrated with respect to the C-1s peak at 285.0 eV, arising from adventitious hydrocarbon on TiO_2. To calculate the stoichiometry of the films, ratios between the areas of the N-1s peaks (395.9 eV) and the Ti-$2p_{3/2}$ peaks (458.7 eV) were taken after subtracting a Shirley background.[42] Scofield sensitivity factors were used for quantification.[43]

The microstructures of the films were analyzed by use of a LEO 1550 scanning microscope with a Gemini column, operating at 5 kV. Images were acquired using an inlens detector. Surface topographies were analyzed by AFM, using a Nanoscope II instrument in tapping mode with an etched silicon cantilever having a tip radius of 10 nm. Data were collected in ambient air with a contact force of about 10^{-7} N. Scans were extended over areas of 2.5 × 2.5 μm^2. Additionally, TEM was carried out using a field emission gun TECNAI F30 ST operated at 300 kV with a point resolution of 2.05 Å. The specimen preparation for TEM followed the procedure described by Gómez et al.[44]

III. Results and Discussion

A. Sputter Deposition of $TiO_{2-x}N_x$ Films. Figure 1 shows that the deposition rate drops from an initial value of 0.29 to 0.14 nm/s as the nitrogen gas flow ratio is increased from zero to 0.025. A small plateau in r appears for Φ values in the range around 0.01. The decrease of r can be ascribed to "poisoning" of the initially metallic target by the formation of oxide layers at low Φ's and nitrides or oxynitrides at large Φ's.

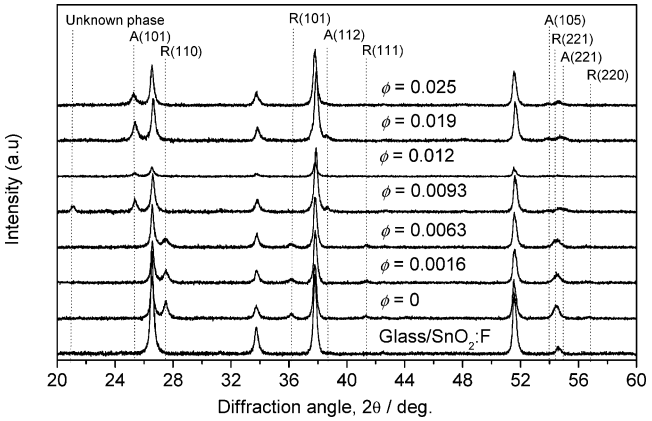

Figure 2. X-ray diffractograms for nitrogen-doped titanium dioxide films prepared using varying values of the nitrogen content Φ in the sputter gas and for a bare substrate. A and R denote anatase and rutile structures, respectively. More restricted XRD data were reported earlier in ref 9.

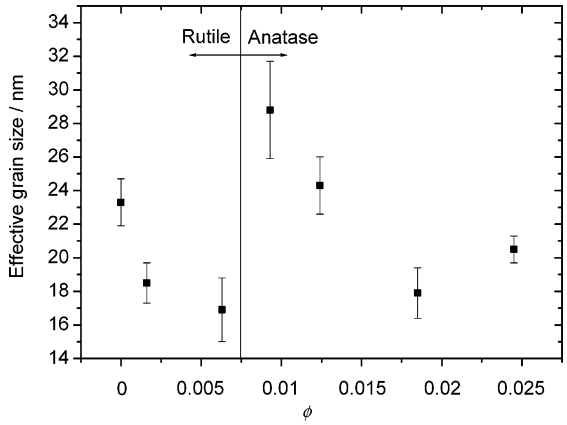

Figure 3. Effective grain size for nitrogen-doped titanium oxide films versus nitrogen content Φ in the sputter plasma. The vertical line indicates the demarcation between different crystal structures.

Figure 2 shows XRD patterns of the films reported in Figure 1, as well as XRD features due to the substrate. Clear evidence of two separate phases can be seen for the TiO_2-type structure, with rutile at $0 < \Phi < 0.007$ and anatase at $\Phi > 0.007$. Thus, the presence of nitrogen seems to induce a rutile-to-anatase transition for the TiO_2-like structure. Although not manifest in the XRD data, we suspect that a mixture of rutile and anatase is present for Φ values being 0.0063 and above. It can be seen in the electron diffractograms—to be presented later in Figure 7—that there are traces of anatase in the dominating rutile structure in the film prepared with $\Phi = 0.0063$. There also seems to exist a crystal mixture in the film sputtered with $\Phi = 0.025$; the crystal structure is mainly anatase, as seen in the X-ray diffractogram in Figure 2, with some traces of rutile as apparent from Figure 7. Selected-area electron diffraction patterns displayed ring features, implying that this film contained more defects than the other films. The anatase−rutile phase transition of TiO_2 has earlier been observed by cation doping[45,46] and also by altering the O_2/Ar gas ratio during reactive magnetron sputtering.[47]

Effective grain sizes, calculated from eq 1, are plotted in Figure 3. The value of L_{eff} is decreased upon nitrogen incorporation within the rutile region, from about 23 to 16 nm for Φ increasing from zero to 0.006. In the range of Φ where *r* displayed a plateau (see Figure 1), one can observe an enhancement of L_{eff} to a value as large as 29 nm. Clearly, this grain size pertains to the transition region between the rutile and anatase phases. Finally, for the largest Φ the effective grain size is increased again. These observed magnitudes of L_{eff} are in the same range as those for other TiO_2 films prepared by sputtering.[21,48]

TABLE 1: Comparison of Crystal Structure, Photoactivity, and Color for Nitrogen-Doped Titanium Dioxide Films, Together with Voltage and Power Used To Maintain the Sputter Plasma[a]

film	crystal structure	photoactivity in visible light	color	min voltage	min power
A	rutile	good	yellow	454 V	342 W
B	rutile + anatase	poor	yellow	445 V	336 W
C	anatase	poor	yellow	420 V	317 W
D	anatase	poor	gray	410 V	310 W

[a] The depositions took place with a nitrogen content of 0.0063 in the sputter plasma.

Sputtering to make nitrogen-doped TiO_2 films is not straightforward. As for sputtering in general, many parameters—such as power, sputtering time, temperature, gas flow ratio, and pressure—need to be carefully controlled and optimized. For the $TiO_{1-x}N_x$ films, it was observed that the power and voltage of the sputter plasma dropped slightly during the depositions, which can be linked to depletion of the target with sputtering time in combination with "poisoning". Table 1 show that the color of the films, as well as their crystal structure, is sensitive to a lowering of the magnitudes of the sputtering parameters. In earlier reports,[9,34] we concluded that the photoelectrochemical response of the sputter-deposited nitrogen-doped TiO_2 films was dependent on their crystal structure. A strong optimum of this response was observed when nitrogen gas was introduced during deposition; the ensuing films corresponded to $\Phi = 0.0063$ and had a mixed crystal structure dominated by rutile TiO_2. The photoactive $TiO_{2-x}N_x$ was obtained for powers and voltages higher than, or equal to, those corresponding to film A in Table 1, when the current was fixed to 0.75 A. If the sputter parameters dropped below the values for film A, a mixed anatase−rutile crystal structure started to evolve (film B). Those films showed very low photoresponse.[9] Eventually, the films turned into complete anatase if the parameters dropped further (film C). Those films were less yellow than the rutile films and showed very low photoactivity.[9] If the parameters kept dropping still further, the yellow color was completely lost, and anatase films having a grayish appearance appeared instead. Moreover, the deposition rate of the nitrogen-doped TiO_2 films also decreased as a consequence of falling sputter parameters.

B. XPS Data. Calibrated XPS measurements showed that all four samples exhibited Ti-$2p_{3/2}$ peaks at 458.7 eV and O-1s peaks at 529.9 eV (data not shown). Figure 4 indicates that the N-1s peaks have two distinct features: a relatively sharp peak at 395.9 eV exhibited by the three N-doped samples and a broad N-1s peak in the region of 399−403 eV obtained in all four samples (including pure TiO_2). The peak at 395.9 eV is attributed to the N-1s signal from atomic nitrogen within $TiO_{2-x}N_x$.[7,10,49−52] Although controversy exists as to the lattice position of N and to the bonding of N within the $TiO_{2-x}N_x$ structure,[49] it is evident from Figure 4 that the N-1s electron emission at 395.9 eV, thought to arise from N-doping, was not observed for the pure TiO_2 sample. In calculating the $TiO_{2-x}N_x$ stoichiometry, only the 395.9 eV peak was used. Compositions with *x* corresponding to 0, 0.010, 0.013, and 0.022 were found for the four films as Φ was increased from zero to 0.025. The compositions are of the same order of magnitude as in the $TiO_{2-x}N_x$ powder synthesized by Irie et al.[10] The film, which earlier proved to be photoelectrochemically very active under

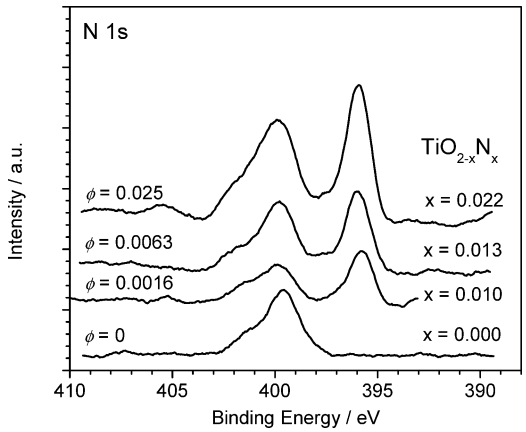

Figure 4. X-ray photoelectron spectra in the N 1s region for nitrogen-doped titanium oxide films deposited with the shown nitrogen contents Φ in the sputter plasma. The curves are vertically displaced.

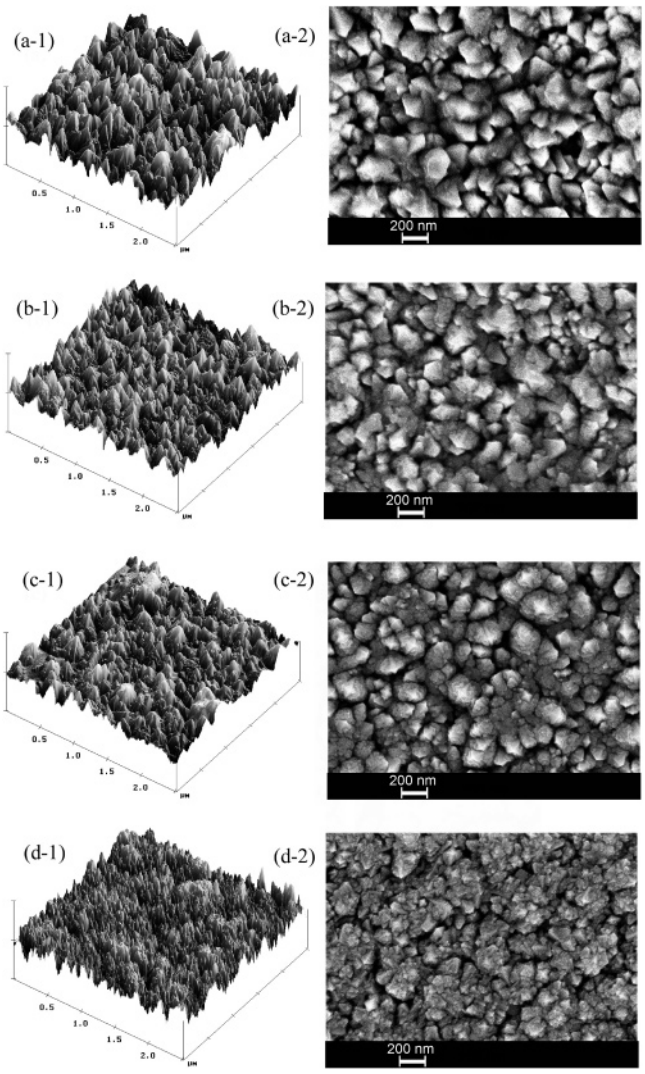

Figure 5. Atomic force microscopy images (left-hand panels, denoted 1) and scanning electron microscopy (SEM) images (right-hand panels, denoted 2) for nitrogen-doped titanium dioxide films. The nitrogen content in the sputter plasma was zero (a), 0.0016 (b), 0.0063 (c), and 0.025 (d). The SEM data were reported earlier in ref 9.

visible light irradiation,[9,34] (prepared with $\Phi = 0.0063$) had a nitrogen content equal to $x = 0.013$ (i.e., 0.65% of the oxygen atoms were replaced by nitrogen atoms).

The origin of the broad peak in the 399−403 eV region is subject to much controversy. Previous work has assigned it to

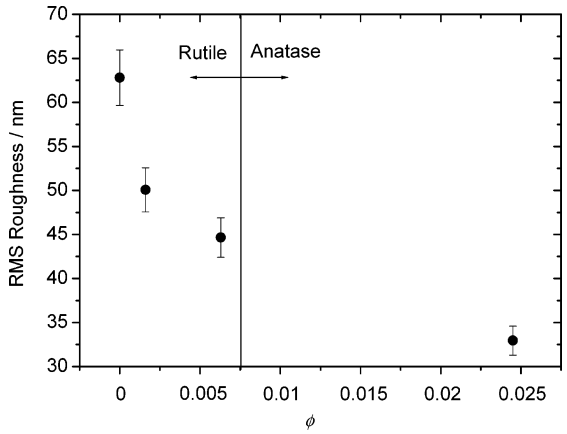

Figure 6. Root-mean-square (RMS) roughness for nitrogen-doped titanium oxide films versus nitrogen content Φ in the sputter plasma. The vertical line indicates the demarcation between different crystal structures.

either adsorbed molecular N_2[7,10,51,52] or interstitial molecular N_2.[49,50] This broad N-1s peak is observed in all four samples, including in pure TiO_2 synthesized in the absence of added nitrogen in the plasma (trace N_2 was present in the Ar and O_2 sources, though). Molecular N_2 does not factor into the stoichiometry of $TiO_{2-x}N_x$, and thus the XPS feature at 399−403 eV was not utilized for stoichiometric quantification. Although we suspect the source of this peak to be interstitial N_2, a conclusive determination of interstitial versus adsorbed N_2, as observed by XPS, is outside the scope of this work; however, further investigation is planned.

C. Morphology and Surface Roughness. AFM and SEM images, depicted in Figure 5, indicate that all films exhibit roughness whose vertical and horizontal extents display similar trends. The linear size of the crystalline nodules decreases with increasing Φ. Our data are in overall agreement with published work.[21] Figure 6 shows that the root-mean-square of the protrusion heights, apparent in the AFM data, decreases with increasing Φ. This roughness is much larger than the effective grain size calculated using Scherrer's formula (cf. Figure 3). A similar observation has been made elsewhere[48] for TiO_2 films; in this earlier work, it was assumed that either the grains were not spherical, or, if they had such shapes, they were largest at the surface of the film.

Figure 7 illustrates TEM images of cross sections through films deposited with four different values of the nitrogen gas ratio. A parallel penniform microstructure[16] can be seen over the full cross sections of the nitrogen-doped TiO_2 films. It is similar to the structure in samples that were previously sputter-deposited under analogous conditions, though without nitrogen addition.[16,21,45] A very large internal surface is manifest, and the ability to have structural contact between, in principle, every part of the surface coating and the underlying substrate makes our films of much interest for applications requiring electrical conductivity (such as solar cells). It can also be seen here that the surface roughness is diminished when the amount of nitrogen, present during sputtering, is increased. We expect that the film porosity has a similar trend.

D. Optical Properties. Optical properties were recorded to complement the structural studies. Solar and luminous transmittance is plotted in Figure 8. These quantities follow the same trend, except for the films deposited without nitrogen. In general, the integrated transmittance values increase upon nitrogen incorporation. In the region where mixed rutile and anatase phases are present, and where a plateau was found in the

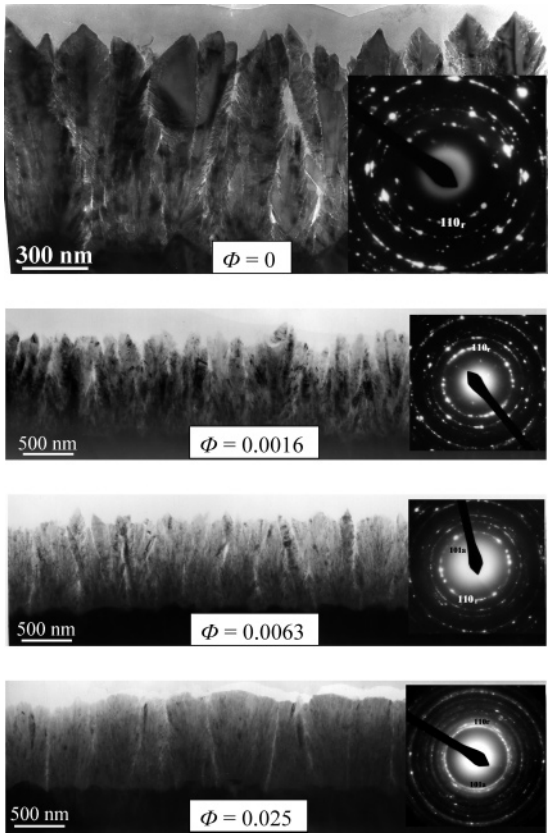

Figure 7. Transmission electron micrographs of cross sections through nitrogen-doped titanium oxide films deposited with the shown nitrogen contents Φ in the sputter plasma. Insets depict electron diffractograms of the films.

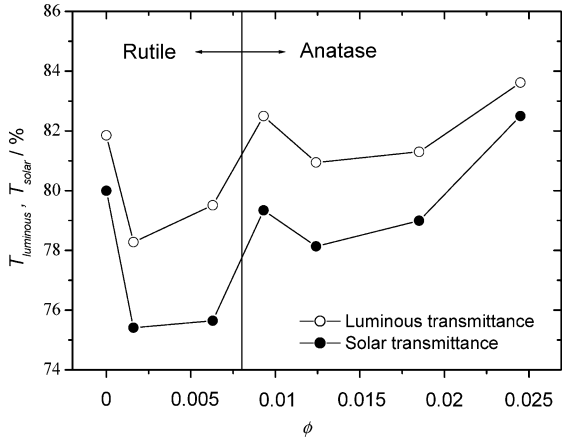

Figure 8. Wavelength-integrated luminous and solar transmittance *T* of nitrogen-doped titanium oxide films versus nitrogen content Φ in the sputter plasma. Dots indicate evaluated data and lines were drawn for convenience. The vertical line indicates the demarcation between different crystal structures.

deposition rate, the solar and luminous transmittance displays large values.

Our nitrogen-doped films have a transparent yellowish color, which is consistent with the appearance of similar films prepared by Asahi et al.[7] Figure 9 shows the absorption coefficient, evaluated using eq 2, plotted as a function of Φ in the $400 < \lambda < 520$ nm wavelength range. Nitrogen doping modifies the absorption of the films so that it extends well into the visible light region and displays a threshold at a wavelength of around 520 nm. The absorption coefficient does not rise as abruptly at 520 nm as it does for undoped TiO_2 at 410 nm. This suggests

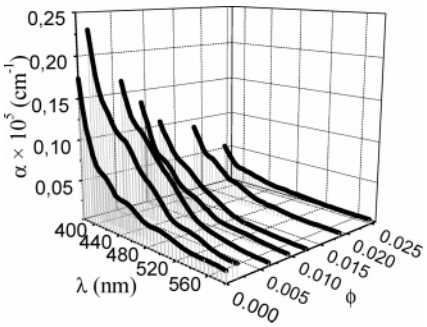

Figure 9. Optical absorption coefficient α as a function of wavelength λ for nitrogen-doped titanium dioxide films prepared with the shown magnitudes Φ of nitrogen in the sputter plasma.

that the new spectral band, in the $410 < \lambda < 535$ nm interval, is not a band-to-band transition but rather is due to excitation of electrons from localized states in the band gap to unoccupied states in the conduction band. Therefore, it is questionable if the term "band gap narrowing", employed by Taga et al.,[7] should be used to describe visible light absorption of nitrogen-doped titanium oxide. The absorption in the wavelength region covered in Figure 9 varies as the amount of nitrogen in the gas mixture is altered. The weak contribution to the absorption spectrum, seen in the visible range for the undoped film, is attributed to scattering rather than absorption in the material. Clearly, α reaches a maximum for Φ lying at about 0.006, that is, when the structure is fine-grained rutile. At larger Φ values, when the anatase structure prevails, the absorption tends to drop. Our observations are consistent with those reported by Lindgren et al.[9] In that report, it was stated that the film that gave the best absorption of light also had the largest photoelectrochemical response. The nitrogen-doped films were photoactive from wavelengths of 520 nm and below.[9]

Currently, we are working on fabricating thicker photoactive films in a search for a film with higher photoelectrochemical response. We are also looking for an explanation to the pronounced optimum of nitrogen incorporation in the photoelectrochemical response.

IV. Conclusions

$TiO_{2-x}N_x$ films were fabricated by reactive DC magnetron sputtering without posttreatment. At low nitrogen contents in the sputter plasma, the films exhibited a rutile structure, while films made at higher nitrogen partial pressures were of anatase type. Thus, the nitrogen incorporation induces a rutile-to-anatase transition. The thin film deposition rate was only weakly dependent on the nitrogen pressure in the transition range, and the grain size was particularly small on the rutile-rich side of the structural transition.

The microstructures of the films were investigated by AFM, SEM, and TEM. The front surface of the TiO_2 films sputtered without nitrogen showed a three-dimensional porous network of interconnected titanium dioxide nodules, each being from 100 to 400 nm in size. The nodules became less and less pronounced as more and more nitrogen was incorporated in the crystal structure. Additionally, transmission electron microscopy was carried out on cross sections of the films. A similar porous parallel penniform microstructure can be seen in the nitrogen-doped TiO_2 as in the samples that were prepared without an addition of nitrogen. However, addition of nitrogen, apart from decreasing the surface roughness, also seemed to diminish the porosity of the films.

The composition of the $TiO_{2-x}N_x$ films was studied with X-ray photoelectron spectroscopy. The magnitude of x rose from zero to 0.022 as the nitrogen gas ratio was increased from zero to 0.025. This corresponds to 1.1% of the oxygen atoms being replaced by nitrogen atoms.

The solar and luminous transmittance increased upon addition of nitrogen to the sputter gas. The appearance of nitrogen-induced absorption at wavelengths between 400 and 520 nm gave the films a transparent yellowish color. This absorption reached a maximum in a range of deposition parameters where the rutile phase prevailed. A further increase of the nitrogen content decreased the absorption within the anatase region.

The present study has shown that the crystal structure, optical properties, and morphology of TiO_2 can be altered by doping with nitrogen, hence opening avenues toward the tailoring of TiO_2-based films for numerous applications, including photoelectric and photochemical ones.[9]

Acknowledgment. We gratefully acknowledge assistance by Judith Kopniczky and Anders Hoel for AFM and SEM measurements, respectively. J. M. Mwabora would like to thank the International Science Program of Uppsala University for a fellowship. E. Avendaño is grateful for a scholarship from the University of Costa Rica to complete the PhD program at Uppsala University. T. F. Jaramillo would like to thank Prof. Eric McFarland and Dr. Tom Mates for fruitful discussions, and the U.S. DOE for partial support under grant #DER-FC36-01G011092. This work made use of the UCSB MRL Central Facilities supported by the U.S. National Science Foundation under award DMR96-32716.

References and Notes

(1) Hagfeldt, A.; Grätzel, M. *Acc. Chem. Res.* **2000**, *33*, 269.
(2) Wang, P.; Zakeeruddin, S. M.; Moser, J. E.; Nazeeruddin, M. K.; Sekiguchi, T.; Grätzel, M. *Nature Mater.* **2003**, *2*, 402.
(3) Sarala Devi, G.; Hyodo, T.; Shimizu, Y.; Egashira, M. *Sens. Actuators, B* **2002**, *87*, 122.
(4) Skryshevsky, V. A.; Vikulov, V. A.; Tretiak, O. V.; Zinchuk, V. M.; Koch, F.; Dittrich, T. *Phys. Status Solidi A* **2003**, *197* (2), 534.
(5) Ohko, Y.; Tatsuma, T.; Fujii, T.; Naoi, K.; Niwa, C.; Kubota, Y.; Fujishima, A. *Nature Mater.* **2002**, *2*, 29.
(6) Rao, K. N. *Opt. Eng.* **2002**, *41* (9), 2357.
(7) Asahi, R.; Morikawa, T.; Ohwaki, T.; Aoki, K.; Taga, Y. *Science* **2001**, *293*, 269.
(8) Ohno, T.; Mitsui, T.; Matsumura, M. *Chem. Lett.* **2003**, *32* (4), 364.
(9) Lindgren, T.; Mwabora, J. M.; Avendaño, E.; Jonsson, J.; Hoel, A.; Granqvist, C. G.; Lindquist, S. E. *J. Phys. Chem. B* **2003**, *107*, 5709.
(10) Irie, H.; Watanabe, Y.; Hashimoto, K. *J. Phys. Chem. B* **2003**, *107* (23), 5483.
(11) Sunada, K.; Watanabe, T.; Hashimoto, K., *J. Photochem. Photobiol., A: Chem.* **2003**, *156*, 227.
(12) Sirghi, L.; Aoki, T.; Hatanaka, Y. *Thin Solid Films* **2002**, *422*, 55.
(13) Stevens, N.; Priest, C. I.; Sedev, R.; Ralston, J. *Langmuir* **2003**, *19*, 3272.
(14) Sirghi, L.; Hatanaka, Y. *Surf. Sci.* **2003**, *530*, L323.
(15) Hagfeldt, A.; Grätzel, M. *Chem. Rev.* **1995**, *95*, 49.
(16) Rodríguez, J.; Gómez, M.; Lu, J.; Olsson, E.; Granqvist, C. G. *Adv. Mater.* **2000**, *12* (5), 341.
(17) Lindström, H.; Holmberg, A.; Magnusson, E.; Malmqvist, L.; Hagfeldt, A. *Nanoletters* **2001**, *1*, 97.
(18) Zeman, P.; Takabayashi, S. *J. Vac. Sci. Technol., A* **2002**, *20*, 388.
(19) Hukari, K.; Dannen, R. *J. Mater. Res.* **2002**, *17*, 550.
(20) Rodríguez, J.; Gómez, M.; Ederth, J.; Niklasson, G. A.; Granqvist, C. G. *Thin Solid Films* **2000**, *365*, 119.
(21) Gómez, M.; Rodríguez, J.; Lindquist, S. E.; Granqvist, C. G. *Thin Solid Films* **1999**, *342*, 148.
(22) O'Regan, B.; Grätzel, M. *Nature* **1991**, *353*, 737.
(23) Anpo, M.; Takeuchi, M. *J. Catal.* **2003**, *216*, 505.
(24) Sato, S. *Chem. Phys. Lett.* **1986**, *123* (1,2), 126.
(25) Morikawa, T.; Asahi, R.; Ohwaki, T.; Aoki, K.; Taga, Y. *Jpn. J. Appl. Phys.* **2001**, *40*, L561.
(26) Fabreguette, F.; Imhoff, L.; Guillot, J.; Domenichini, B.; Lucas, M. C. M.d.; Sibillot, P.; Bourgeois, S.; Sacilotti, M. *Surf. Coat. Technol.* **2000**, *125*, 396.
(27) Lee, D. H.; Cho, Y. S.; Yi, W. I.; Kim, T. S.; Lee, J. K.; Jung, H. J. *Appl. Phys. Lett* **1995**, *66* (7), 815.
(28) Pradhan, S. K.; Reucroft, P. J. *J. Cryst. Growth* **2003**, *250*, 588.
(29) Makino, Y.; Nose, M.; Tanaka, T.; Misawa, M.; Tanimoto, A.; Nakai, T.; Kato, K.; Nogi, K. *Surf. Coat. Technol.* **1998**, *98*, 934.
(30) Martev, I. N. *Vacuum* **2002**, *67*, 261.
(31) Bittar, A.; Cochrane, D.; Caughley, S.; Vickeridge, I. *J. Vac. Sci. Technol., A* **1997**, *15* (2), 223.
(32) Guillot, J.; Jouaiti, A.; Imhoff, L.; Domenichini, B.; Heintz, O.; Zerkout, S.; Mosser, A.; Bourgeois, S. *Surf. Interface Anal.* **2002**, *34*, 577.
(33) Hukari, K.; Dannenberg, R.; Stach, E. A. *J. Mater. Res.* **2002**, *17* (3), 550.
(34) Lindgren, T.; Romualdo Torres, G.; Lu, J.; Granqvist, C. G.; Lindquist, S. E. *Sol. Energy Mater. Sol. Cells* **2004**, *84*, 145.
(35) Ihara, T.; Miyoshi, M.; Iriyama, Y.; Matsumoto, O.; Sugihara, S. *Appl. Catal., B: Environmental* **2003**, *42*, 403.
(36) Sakthivel, S.; Kisch, H. *ChemPhysChem* **2003**, *4*, 487.
(37) G. Romualdo Torres, G.; Lindgren, T.; Lu, J.; Granqvist C.-G.; Lindquist, S.-E. *J. Phys. Chem. B* **2004**, *108*, 5995.
(38) Le Bellac, D.; Niklasson, G. A.; Granqvist, C.-G. *J. Appl. Phys.* **1995**, *77*, 6145.
(39) Cullity, B. D. *Elements of X-ray Diffraction*; Addison-Wesley: Reading, MA, 1959.
(40) MacAdam, D. L. *Color Measurement: Theme and Variations*; Springer-Verlag: Berlin, 1981.
(41) Hong, W. Q. *J. Phys. D: Appl. Phys.* **1989**, *22*, 1384.
(42) Shirley, D. A. *Phys. Rev. B* **1972**, *5*, 4709.
(43) Scofield, J. H. *J. Electron Spectrosc. Relat. Phenom.* **1976**, *8*, 129.
(44) Gomez, M. M.; Lu, J.; Solis, J. L.; Olsson, E.; Hagfeldt, A.; Granqvist, C. G. *J. Phys. Chem. B* **2000**, *104*, 8712.
(45) Arroyo, R.; Còrdoba, G.; Padilla, J.; Lara, V. H. *Mater. Lett.* **2002**, *54*, 397.
(46) Moon, J.; Takagi, H.; Fujishiro, Y.; Awano, M. *J. Mater. Sci* **2001**, *36*, 949.
(47) Gómez, M. M.; Beermann, N.; Lu, J.; Olsson, E.; Hagfeldt, A.; Niklasson, G. A.; Granqvist, C. G. *Sol. Energy Mater. Sol. Cells* **2003**, *76*, 37.
(48) Mardare, D.; Rusu, G. I. *Analele Stiintifice Ale Universitatii "AL. I. CUZA" IASI, s Fizika Starii Condensate* 1999−2000, *XLV-XLVI*, 201.
(49) Esaka, F.; Furuya, K.; Shimada, H.; Imamura, M.; Matsubayashi, N.; Sato, T.; Nishijima, A.; Kawana, A.; Ichimura, H.; Kikuchi, T. *J. Vac. Sci. Technol., A* **1997**, *15*, 2521.
(50) Esaka, F.; Shimada, H.; Imamura, M.; Matsubayashi, N.; Sato, T.; Nishijima, A.; Kawana, A.; Ichimura, H.; Kikuchi, T.; Furuya, K. *Thin Solid Films* **1996**, *281−282*, 314.
(51) Saha, N.; Tompkins, H. *J. Appl. Phys.* **1992**, *72*, 3072.
(52) Shinn, N. D.; Tsang, K.-L. *J. Vac. Sci. Technol., A* **1991**, *9*, 1558.